UDC 629.5.017.2:629.5.563

Young MYUNG CHOI[1]
Sun HONG KWON[1]
Jung HO PARK[1]
Sang BEOM LEE[1]
Sime MALENICA[2]
Byeong HOON JUNG[3]

Application of Multipole Expansions to Roll Damping

Authors' addresses (Adrese autora):

[1] *Pusan National University*, Busandaehak-ro, 63beon-gil, Geumjeong-gu, Busan, Korea; holohoo123@pusan.ac.kr; shkwon@pusan.ac.kr; hippo@pusan.ac.kr; lsb7766@pusan.ac.kr

[2] *Bureau Veritas*; 92571 Neuilly-Sur –Seine Cdx-France; sime.malenica@bureauveritas.com

[3] *Hyundai Heavy Industry*; 1000, Bangeijinsunhwan-doro, Doog-gu, Ulsan, Korea; bhjung@hhi.co.kr

Received (Primljeno):2012-11-07
Accepted (Prihvaćeno: 2012-11-23
Open for discussion (Otvoreno za raspravu): 2014-06-30

Review paper

This study presents the application of multipole expansion to calculate the roll damping of the rectangular box. The *N*-parameter Lewis form was used to follow the rectangular cross section. The Ursell-Tasai method was employed to deal with non-circular cross section. The added mass and damping coefficient of the sway, heave, and roll motion were calculated. BEM code was developed to compare with the results. Experiment was done to verify the flow field calculated from the multipole expansions.

Keywords: *added mass coefficient, damping coefficient, Lewis form, multipole expansions, roll damping*

Primjena metode multipola na proračun prigušenja ljuljanja

Pregledni znanstveni rad

Ovim radom prikazana je primjena metode multipola na proračun prigušenja zbog ljuljanja prizmatičnoga pontona. Pravokutni poprečni presjek pontona opisan je *N*-parametarskom Lewisovom formom. Metoda Ursella i Tasaia primijenjena je na poprečne presjeke koji nisu kružnog oblika. Izračunati su hidrodinamički koeficijenti dodane mase i radijacijskoga prigušenja za zanošenje, poniranje i ljuljanje. Rezultati su uspoređeni s posebno razvijenim računalnim kodom utemeljenim na metodi rubnih elemenata. Radi potvrde polja strujanja izračunatog na temelju metode multipola provedeno je i eksperimentalno istraživanje.

Ključne riječi: *koeficijent pridružene mase, koeficijent prigušenja, Lewisova forma, metoda multipola, prigušenje ljuljanja*

1 Introduction

Multipole expansions express the velocity potential as a sum of singularities. The singularities are located within a body. The coefficients of the singularities can be obtained imposing boundary conditions on the body when the boundary of the body coincides with the coordinate surfaces [1]. When the boundary of the body deviates from the coordinate surfaces the body boundary should be transformed to match the coordinate surfaces [2]. An attempt to apply multipole expansion to general body has been done by Eatock Taylor and Hu [3]. They applied boundary integral expression to inner fluid domain closed to body and matched multipole expansion at the outside of inner domain. They confirmed only two-dimensional hydrodynamic problem. Mavrakos and Chatjigeorgiou provided the analytic solution for hydrodynamic diffraction problem on submerged prolate spheroids in infinite water depth [4]. The solution method is based on the multipole expansions and employs the multipole potentials derived by Thorn [5].

This study presents the application of multipole expansion to the prediction of roll damping of a box barge. The cross section of the box barge is a rectangular shape. The lower corner of the rectangle has the strong mathematical singularity. To deal with these corners in detail a multiple parameters Lewis form has been adopted. By increasing the parameters of the Lewis form the deviation of the rectangular shape with the conformal mapped body shape decreased. The multipole expression is mapped into unit circle to satisfy the body boundary condition. The coefficients of the multipoles can be determined. Since the velocity potential is known, we can calculate added moment, and damping moment of roll motion can be obtained. To confirm the results, an experiment was carried out. The flow field was recorded with high speed camera. The velocity field was obtained through PIV analysis. The computed and the experimental results are mutually compared.

2 Multipole expansions

Let the fluid be inviscid and incompressible and let it satisfy the requirements for irrotational flow. The depth of the fluid is assumed to be infinite. If the fluid has the harmonic behaviour, the time dependence velocity potential can be introduced in the form $\Phi(\underline{x},t) = \mathrm{Re}[\phi(\underline{x})e^{i\omega t}]$, with the angular frequency ω of fluid domain and oscillating body.

For the two-dimensional problem, we can introduce the Cartesian coordinates Oxz. The z-axis is opposite to the direction of gravitational force acting with the origin O on the mean free-surface and the x-axis is lying on the mean free surface. A submerged or floating body in the fluid oscillates with the angular frequency ω. The governing equation and boundary condition of the problem can be written as follows:

$$\nabla^2\phi = 0 \qquad \text{in} \qquad \text{fluid domain} \tag{1}$$

$$\frac{\partial\phi}{\partial z} = 0 \qquad \text{as} \qquad z \to -\infty \tag{2}$$

$$\frac{\partial\phi}{\partial z} - K\phi = 0 \qquad \text{on} \qquad z = 0 \tag{3}$$

$$\frac{\partial\phi}{\partial n} = \mathbf{V}\cdot\mathbf{n} \qquad \text{on} \qquad \text{body surface} \tag{4}$$

$$\lim_{Kx\to\pm\infty}\left(\frac{\partial\phi}{\partial x}\mp iK\phi\right)=0 \tag{5}$$

The normal vector **n** is pointing out of the fluid. And the wave number K is given by $K=\omega^2/g$ where g is the gravitational acceleration.

2.1 Ursell's multipole expansions

The analytic solution of a heaving and swaying circle in the water is announced by Ursell [1]. He introduced some singularities on the centre of the circle satisfying the Laplace equation, infinite bottom condition, free surface boundary condition and radiation condition except the body boundary condition. He suggested that the total velocity potential can be expressed with the sum of singularities.

$$\phi = A_0 c_0 + \sum_{m=1}^{\infty}\left[A_m c_m + B_m s_m\right] \tag{6}$$

where

$$c_0 = \ln\frac{r'}{r} + 2P.V.\int_0^{\infty}\frac{e^{k(z+f)}}{k-K}\cos kx\,dk \tag{7}$$

$$s_1 = a\left\{\frac{\sin\theta}{r}+\frac{\sin\theta'}{r'}+2kP.V.\int_0^{\infty}\frac{e^{k(z+f)}}{k-K}\sin kx\,dk\right\} \tag{8}$$

$$c_m = a^m\left[\frac{\cos m\theta}{r^m}+\frac{\cos m\theta'}{r'^m}+\frac{K}{m-1}\left(\frac{\cos(m-1)\theta}{r^{m-1}}-\frac{\cos(m-1)\theta'}{r'^{m-1}}\right)\right] \tag{9}$$

$$s_m = a^m\left[\frac{\sin m\theta}{r^m}+\frac{\sin m\theta'}{r'^m}+\frac{K}{m-1}\left(\frac{\sin(m-1)\theta}{r^{m-1}}-\frac{\sin(m-1)\theta'}{r'^{m-1}}\right)\right] \tag{10}$$

In case of a submerged cylinder, let the centre of the cylinder be located at $y=f$. Then the singularities can be expressed as equations (7) to (10). Figure 1 depicts the coordinate system and the location of singularities. Above potentials in equations (9) to (10) do not make the waves at the infinity. They decay to zero as $x\to\pm\infty$. In other words, they are involved in local disturbance near the body. So the potentials representing outgoing waves at infinity are also needed to satisfy the radiation condition written in equations (7) to (8). The wave potential in equation (7) is the pulsating source potential. Wave potentials in equations (7) to (8) can be expressed in terms of exponential integral $E_1(Z')$ [6].

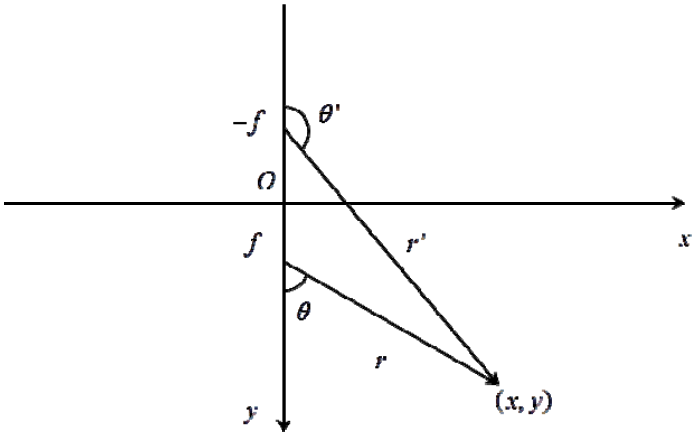

Figure1 **Description of coordinate system**
Slika 1 **Definicija koordinatnog sustava**

$$c_0 = \ln\frac{r'}{r} + 2\left\{\mathrm{Re}\left[e^{Z'}E_1(Z')\right] - \pi i e^{K(f+z)-iK|x|}\right\} \tag{11}$$

$$s_1 = a\left\{\frac{\sin\theta}{r} + \frac{\sin\theta'}{r'} + 2k\left[\mathrm{Im}\left[e^{Z'}E_1(Z')\right] + \mathrm{sgn}(x)\pi e^{K(f+z)-iK|x|}\right]\right\} \tag{12}$$

where

$$Z' = K(z+f+ix) = Kr'e^{i\theta'}$$

At the infinity, $\ln r'/r$ and $e^{Z'}E_1(Z')$ go to zero. If the circle is floating on the free surface with *f=0*, then the multipoles are simply represented.

$$c_0 = 2\,\mathrm{Re}\left[e^{Z'}E_1(Z')\right] - 2\pi i e^{K(f+z)-iK|x|} \tag{13}$$

$$s_1 = a\left\{\frac{\sin\theta}{r} + 2K\left[\mathrm{Im}\left[e^{Z'}E_1(Z')\right] + \mathrm{sgn}(x)\pi e^{K(f+z)-iK|x|}\right]\right\} \tag{14}$$

$$c_{2m} = 2a^{2m}\left[\frac{\cos m\theta}{r^{2m}} + \frac{K}{2m-1}\frac{\cos(2m-1)\theta}{r^{2m-1}}\right] \tag{15}$$

$$s_{2m+1} = a^{2m+1}\left[\frac{\sin(2m+1)\theta}{r^{2m+1}} + \frac{K}{2m}\frac{\sin 2m\theta}{r^{2m}}\right] \tag{16}$$

The other terms are zero. To determine the coefficients of the potential, we can define the radiation potential ϕ_j by $\Phi = \mathrm{Re}[i\omega\xi_j\phi_j e^{i\omega t}]$ which has the velocity of unit amplitude in the *j* th mode. From the body boundary condition we can determine the coefficient.

$$\sum_{m=1}^{N} B_m \frac{\partial s_m}{\partial n} = \sin\theta \qquad \text{on} \qquad r = a\text{, Sway} \tag{17}$$

$$A_0\frac{\partial c_0}{\partial n} + \sum_{m=1}^{N-1} A_m \frac{\partial c_m}{\partial n} = \cos\theta \qquad \text{on} \qquad r = a\text{, Heave} \tag{18}$$

This problem was first solved by Ursell and complete results were given by Ogilvie [1,7,8].

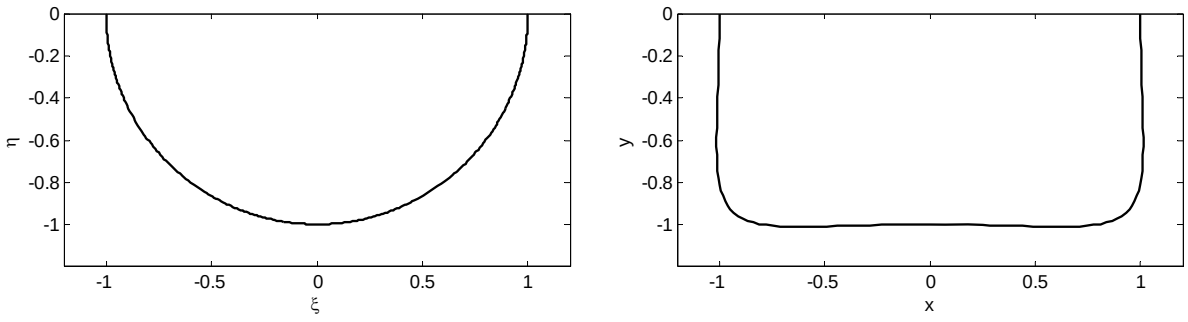

(a) Unit Circle (ζ – plane) **(b) Transformed 3-parameter Lewis form (z – plane)**

Figure 2 **Description of geometric plane (z -plane) and transform plane (ζ -plane)**
Slika 2 **Geometrijska ravnina (*z*-ravnina) i ravnina transformacije (ζ -ravnina)**

2.2 Conformal mapping

Ursell's multipole expansion is restricted to the circular circle only. However, a ship has more complex geometry which is hard to be expressed analytically. Ship's middle section shape is similar to a rectangle. Tasai computed the complex geometry by introducing the conformal mapping function [2].

$$z = M\sum_{n=0}^{N} a_{2n-1}\zeta^{2n-1} \qquad \text{where} \qquad z = x + iy\,, \quad \zeta = re^{i\theta} \tag{19}$$

The position vector of the body surface is defined in the *z*-plane. Using the conformal mapping function the position vector describing the surface of the body can be expressed in the ζ-plane (see Figure 2 (a) and (b)). A very simple transformation of cross sectional hull form is obtained *N=2* in the conformal mapping function which is the Lewis transformation [9].

$$z = M\left(\zeta + \frac{a_1}{\zeta} + \frac{a_3}{\zeta^3}\right) \tag{20}$$

where

$$a_1 = \frac{H_0 - 1}{2(M/d)} \quad \text{and} \quad a_3 = \frac{H_0 + 1}{2(M/d)} - 1 \tag{21}$$

with the hull form factor

$$M = \frac{B/2}{1 + a_1 + a_3}, \quad H_0 = \frac{B/2}{D} \quad \text{and} \quad \sigma = \frac{A}{BD} = \frac{\pi}{4}\frac{1 - a_1^2 - 3a_3^2}{(1 + a_3)^2 - a_1^2} \tag{22}$$

where

$$\frac{M}{d} = \frac{3(H_0 + 1) - \sqrt{(H_0 + 1)^2 + 8H_0(1 - 4\sigma/\pi)}}{4} \tag{23}$$

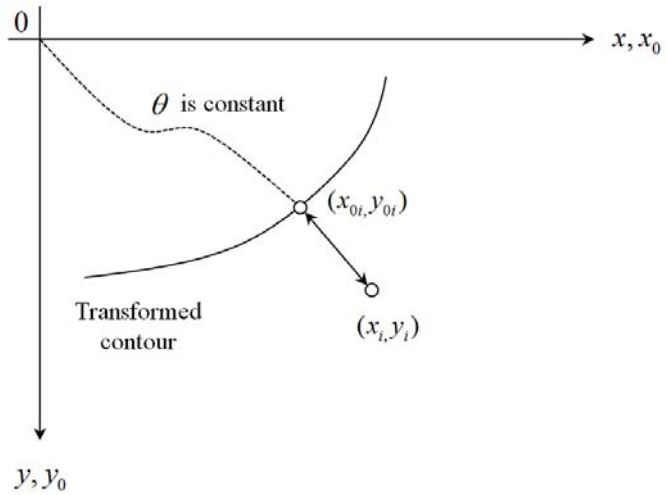

Figure 3 ***N*- parameter Lewis form**
Slika 3 ***N*- parametarska Lewisova forma**

The coefficients in the mapping function are determined with the hull form factor. H_0 and σ represent the ratio of half breadth and draft and area coefficient. So far we have looked over the simple Lewis form which is determined with the ratio of half breadth and draft and area coefficient. But in case when the body shape is arbitrary, the 3-parameter Lewis form is not suitable to express the arbitrary body shape. So we applied the *N*-parameter conformal mapping function to express an arbitrary body shape. To determine the coefficients in the formula, we used the information of the offset point on the body surface. The contour of the approximate cross section is given by increasing the number of parameters.

$$x_0 = -M\sum_{n=0}^{N}(-1)^n a_{2n-1}\sin(2n-1)\theta \tag{24}$$

$$y_0 = +M\sum_{n=0}^{N}(-1)^n a_{2n-1}\cos(2n-1)\theta \tag{25}$$

If θ is determined with the offset, we can define the error with the numerical value of the square of the deviation of (x_i, y_i) from (x_{0i}, y_{0i}) which is shown in Figure 3.

$$E = \sum_{i=o}^{I} e_i \tag{26}$$

where

$$e_i = (x_i + \sum_{n=0}^{N}\{(-1)^n[M\cdot a_{2n-1}]\sin((2n-1)\theta_i)\})^2 + (y_i - \sum_{n=0}^{N}\{(-1)^n[M\cdot a_{2n-1}]\cos((2n-1)\theta_i)\})^2$$

Then the new values of $M \cdot a_{2n-1}$ have to be obtained in such a manner that E is minimized.

$$\frac{\partial E}{\partial(M\cdot a_{2j-1})} = 0 \qquad \text{for} \quad j = 0,1,\cdots,N \tag{27}$$

This yields *N+1* equations, but derived the equations do not satisfy the exact breadth and draft. To obtain the exact breadth and draft, the last two equations are replaced by the equations for the breadth at the water line and the draft.

$$\sum_{n=0}^{N}\left[(-1)^n M\cdot a_{2n-1}\right]\sum_{i=0}^{I}\cos(2j-2n)\theta_i = \sum_{i=0}^{I} -x_i\sin(2j-1)\theta_i + y_i\cos(2j-1)\theta_i$$

$$\text{for} \qquad j = 0,\cdots,N-2 \tag{28}$$

$$\sum_{n=0}^{N}[M\cdot a_{2n-1}] = B/2 \qquad \text{for} \qquad j = N-1 \tag{29}$$

$$\sum_{n=0}^{N}\left[(-1)^n M\cdot a_{2n-1}\right] = d \qquad \text{for} \qquad j = N \tag{30}$$

These *N+1* equations can be solved by a numerically iterative method. The advantage of using the *N*-parameter Lewis form is that we can get the approximated mathematical formula describing the hull form using the information of the hull's offset. However, the disadvantage is that we need to compute the coefficients by a numerically iterative method. Figure 4 shows

that as the parameter increases, the improvement gets better. The error decreases as the number of iteration increases, as shown in Figure 5.

2.3 Ursell-Tasai method

In the previous chapter, we introduced the *N*-parameter Lewis form. Tasai expressed the multipole expansion by introducing the 3-parameter Lewis form [2]. But the 3-parameter Lewis form has the disadvantages to describe the arbitrary body shape as shown earlier. To overcome this disadvantage, we expanded the Tasai's multipole expansion expressed with the 3-parameter to the *N*- parameter multipole expansion.

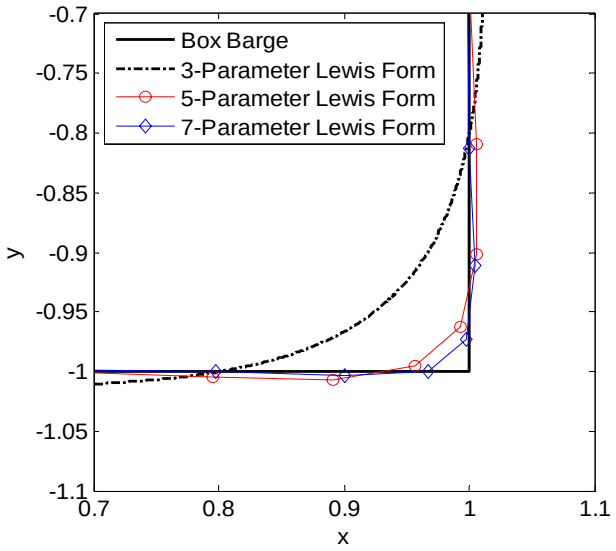

Figure 4 **N - parameter Lewis form with N increments**
Slika 4 **N - parametarska Lewisova forma u ovisnosti o broju parametara**

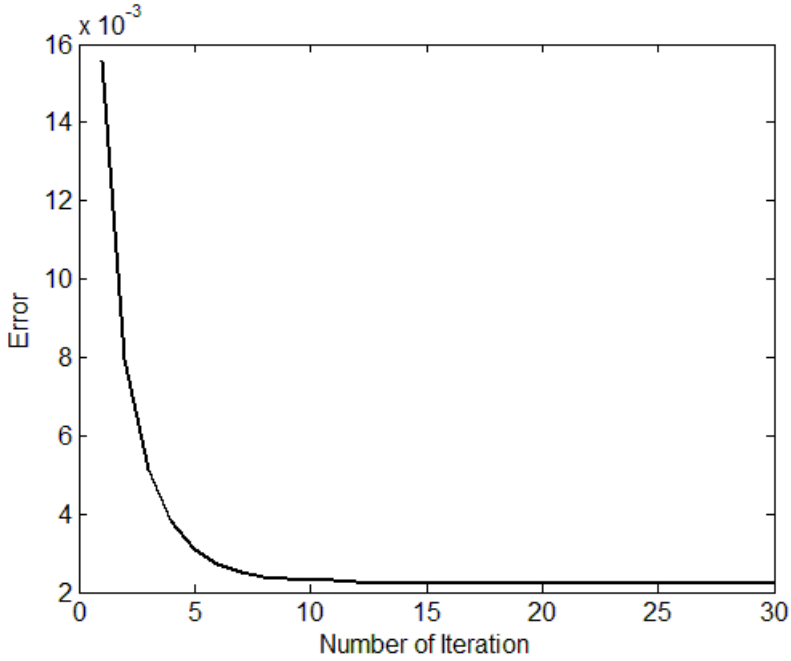

Figure 5 **Convergence of the offset error**
Slika 5 **Konvergencija greške u opisu pravokutnog presjeka**

2.4 Symmetric motion (heave)

For the symmetric motion like heave, the multipole expansion is written as equations (31) to (32).

$$\Phi(x,y,t) = \mathrm{Re}\left[i\omega X_2 \phi_S(x,y) e^{i\omega t} \right] \tag{31}$$

$$\phi_S = A_0 \left[\phi_{c0}^S + i\phi_{s0}^S \right] + \sum_{m=1}^{\infty} A_{2m} \phi_{2m}^S \tag{32}$$

Since the motion is symmetric, the flow also has symmetric behaviour. The components of multipole expansion for symmetric motion have the forms below. The two dimensional infinite Green function is also shown in equation (33).

$$\begin{aligned} \phi_{c0}^S + i\phi_{s0}^S &= 2 \lim_{\mu \to 0} \int_0^{\infty} \frac{e^{-ky} \cos kx}{k - K + i\mu} dk \\ &= 2 \left[P.V. \int_0^{\infty} \frac{e^{-Ky} \cos Kx}{k - K} dk - \pi i e^{-Ky} \cos Kx \right] \\ &= 2 \left[\int_0^{\infty} \frac{k \cos ky - K \sin ky}{k^2 + K^2} e^{-k|x|} dk - \pi i e^{-Ky - iK|x|} \right] \end{aligned} \tag{33}$$

$$\phi_{2m}^S = \frac{\cos 2m\theta}{r^{2m}} + KM \sum_{n=0}^{\infty} (-1)^{n+1} \frac{(2n-1) a_{2n-1} \cos(2m + 2n - 1)\theta}{(2m + 2n - 1) r^{2m+2n-1}} \tag{34}$$

In here, we can see that the components of the multipole expansion have symmetric behaviour with respect to θ=0.

2.5 Asymmetric motion (sway and roll)

For the asymmetric motions like sway and roll, the multipole expansion can be written as equations (35) to (38). On the contrary to symmetric motion, we can see that the components have asymmetric behaviour with respect to θ=0.

$$\Phi(x,y,t) = \mathrm{Re}\left[i\omega X_{2,3} \phi_A(x,y) e^{i\omega t} \right] \tag{35}$$

$$\phi_A = B_0 \left[\phi_{c0}^A + i\phi_{s0}^A \right] + \sum_{m=1}^{\infty} B_{2m} \phi_{2m}^A \tag{36}$$

$$\phi_{c0}^A + i\phi_{s0}^A = \mp \int_0^2 \frac{k \sin ky + K \cos ky}{k^2 + K^2} e^{-k|x|} dk + \frac{2}{K} \frac{\sin\theta}{r} \pm 2\pi e^{-Ky - iK|x|} \tag{37}$$

$$\phi_{2m}^A = \frac{\sin(2m+1)\theta}{r^{2m+1}} + KM \sum_{n=0}^{\infty} (-1)^{n+1} \frac{(2n-1) a_{2n-1} \sin(2m + 2n)\theta}{(2m + 2n) r^{2m+2n}} \tag{38}$$

The coefficients A_{2m} and B_{2m} in the velocity potential are determined by satisfying the body boundary condition, while the $M \cdot a_{2n\text{-}1}$ is previously determined using the information on the body geometry offset by solving equations (28) to (30).

3 Experiments

In order to measure the velocity field around the box barge forced roll motion was applied. The centre of roll motion was located at the centre of breadth and on the mean free surface. The PIV measurement apparatus was installed to measure the velocity field around the body.

Table 1**Specifications of the model**
Tablica 1 **Značajke modela**

Box Barge Model	
$L \times B \times D$	610 X 300 X 250 (mm)
Draft (d)	150 mm
Material	Acrylic Plastic
Centre of rotation is located 150 mm above the bottom of the model.	

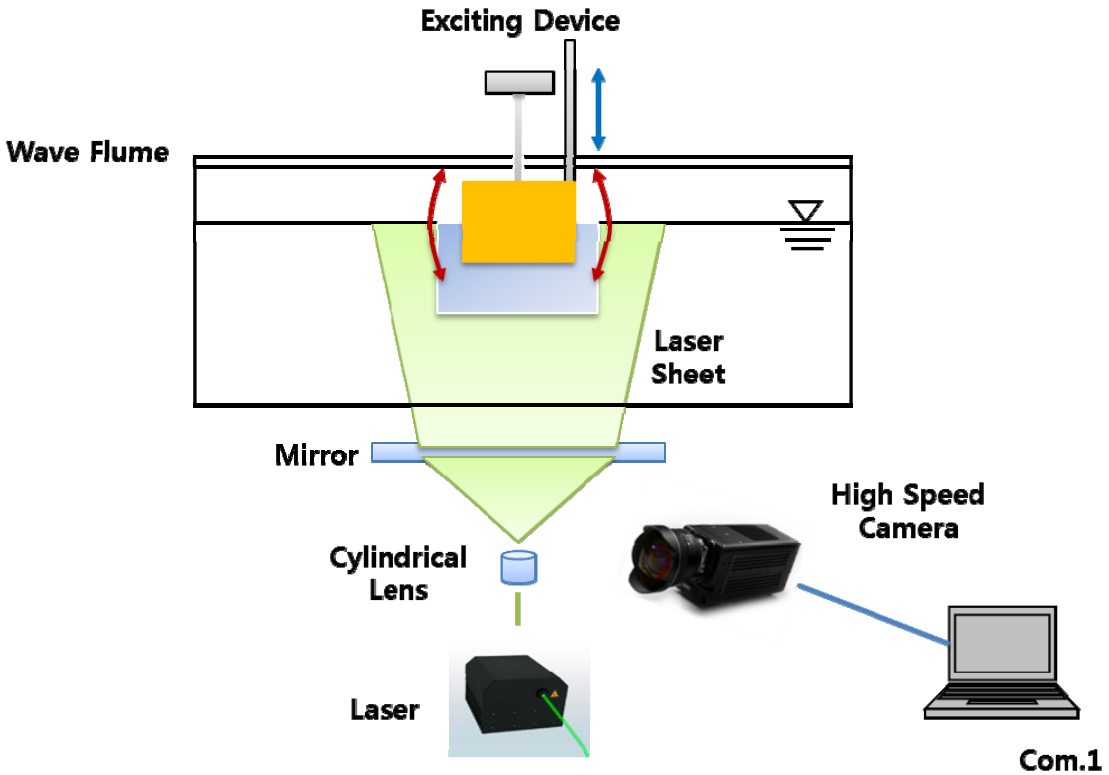

Figure 6 **Description of forced roll motion experiment**
Slika 6 **Prikaz instrumentacije za eksperimente prisilnog ljuljanja**

Figure 7 **Box barge model**
Slika 7 **Model prizmatičnog pontona**

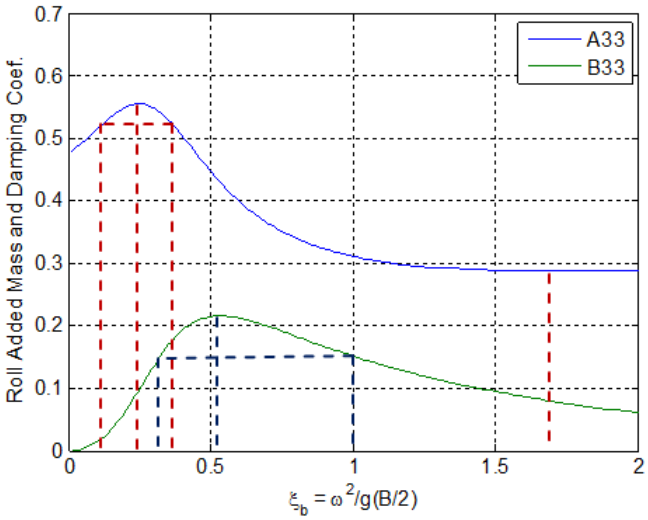

Figure 8 **Selection of test cases based on BEM**
Slika 8 **Odabir testnih primjera na temelju proračuna metodom rubnih elemenata**

Table 2 **Test cases with various Kb**
Tablica 2 **Testni primjeri za različiti Kb**

	$Kb \quad b = 0.15m$
Added Mass Coefficient Comparison	0.10
	0.25
	0.38
Damping Coefficient Comparison	0.32
	0.53
	1.00
	1.75

Figure 6 depicts the schematic view of roll motion. The vertical movement of the servo motor generates roll motion through jig. The laser sheet was generated around the cross section of the body. The high speed camera captured the velocity field around the body. The principal dimensions of the box barge are shown in Table 1. The shape of the box model is presented in Figure 7. To define the test conditions the boundary element analysis was done

on a two dimensional box barge to get hydrodynamic coefficients. The results are shown in Figure 8. The normalized wave numbers at which the added mass and damping coefficients are maxima were selected. Two extra points in between the maxima were selected so that we can observe what happens around the maximum normalized wave number. The selected *Kb* values are presented in Table 2.

4 Analysis and results

Once we got velocity potential expressed in multipole expansion we can obtain hydrodynamic coefficients by integrating the pressure over the surface of the rectangular box.

$$a_{ij} - ib_{ij} / \omega = -\rho \int_{S_H} \phi_j(x,y) n_i dS \tag{39}$$

The normalized hydrodynamic coefficients can be written as

$$a_{ij}^{'} - ib_{ij}^{'} = \frac{a_{ij}}{\rho b^2 \varepsilon_i \varepsilon_j} - i \frac{b_{ij}}{\rho \omega b^2 \varepsilon_i \varepsilon_j} \tag{40}$$

when $j=1,2$ $\varepsilon_j=1$,when $j=3$ then $\varepsilon_j=b$. The hydrodynamic coefficients obtained from equation (40) are presented in Figures 9 to 14. When it comes to the sway motion of the box barge, the hydrodynamic coefficients using the 3-prameter Lewis form expansion were very close to the results calculated by the boundary element method shown in Figures 9 to 10. The same tendency can be verified with the heave motion of the box barge, which can be seen in Figure 11. Better accuracy can be noticed with the added mass than in the case of damping. The added mass and damping coefficients for sway and heave converge very fast and these characteristics are featured in Figures 9 and 12. For the swaying and heaving motion, the convergence of the hydrodynamic coefficients is very fast and shows good results when *N* is small. Hydrodynamic coefficients come from the integration of the pressure of the hull. From Figures 9 to 12, for the sway and heave motion, the pressure at the side wall and bottom is much more dominant than the pressure acting on the corner.

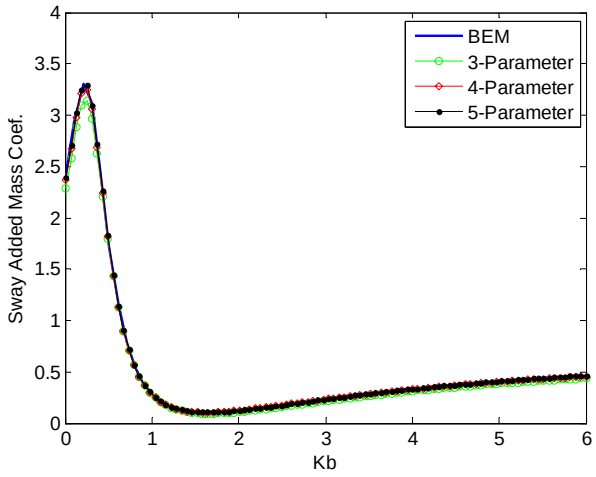

Figure 9 **Convergence of sway added mass**
Slika 9 **Konvergencija dodane mase za zanošenje**

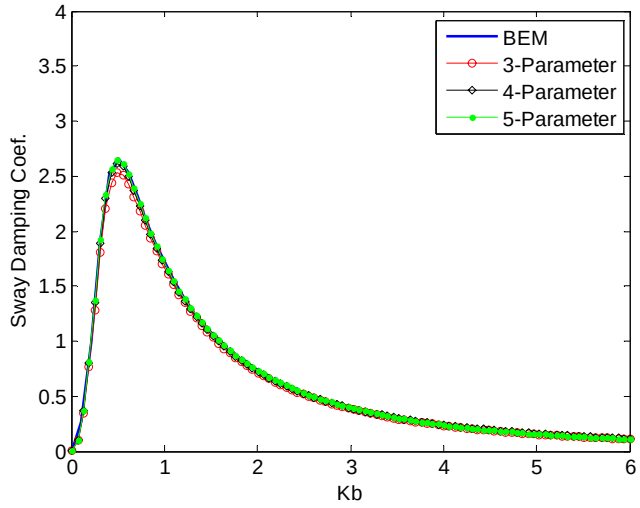

Figure 10 **Convergence of sway damping coefficients**
Slika 10 **Konvergencija radijacijskog prigušenja za zanošenje**

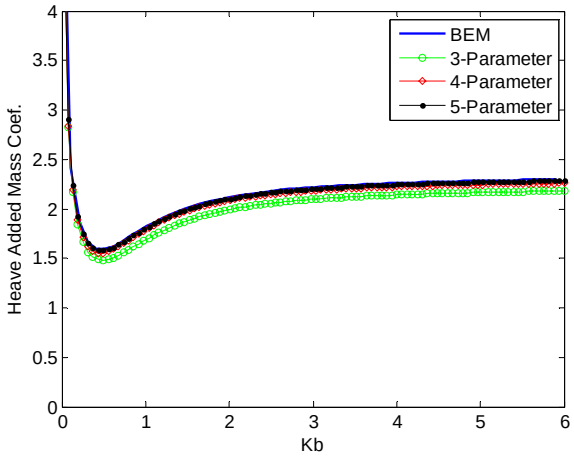

Figure 11 **Convergence of heave added mass**
Slika 11 **Konvergencija dodane mase za poniranje**

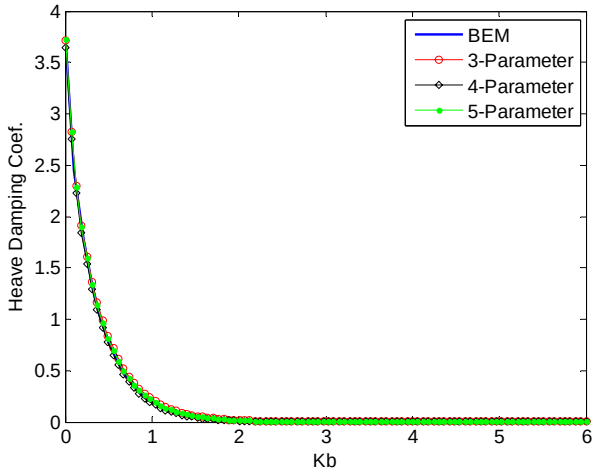

Figure 12 **Convergence of heave damping coefficients**
Slika 12 **Konvergencija radijacijskog prigušenja za poniranje**

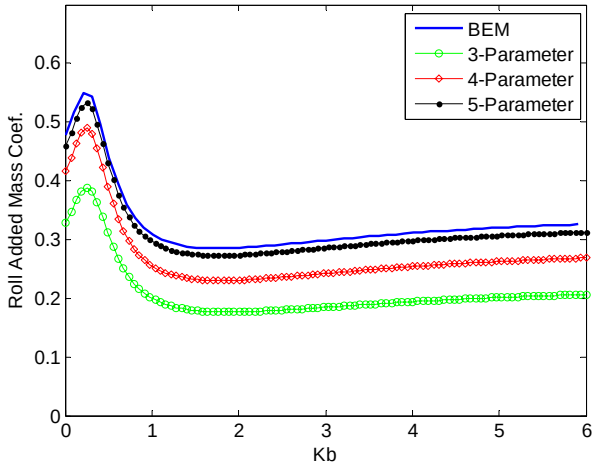

Figure 13 **Convergence of roll added mass**
Slika 13 **Konvergencija dodane mase za ljuljanje**

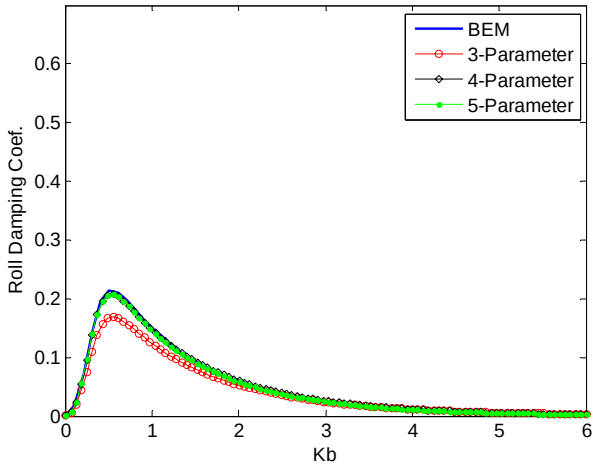

Figure 14 **Convergence of roll damping**
Slika 14 **Konvergencija radijacijskog prigušenja za ljuljanje**

The added mass and damping coefficients of roll motion are very sensitive to the variation of *N*. An increase of only few terms of *N* made big difference in the added mass and damping coefficients, which can be seen in Figures 13 and 14. This means that the pressure acting on the corner of the rectangular barge has significant portion. The deviation from the results of BEM got decreased significantly. The consistence of the numerical code was verified by comparing the amplitude of the wave at infinite region with the damping [10]. The damping coefficient of roll damping at infinite region can be written as equation (41).

$$b_{33} = \rho\omega(\pi |B_0| B_0)^2 \tag{41}$$

The result is shown in Figure 15. The two curves are almost identical. As the value of N increases, the deviation from the result of equation (41) decreased.

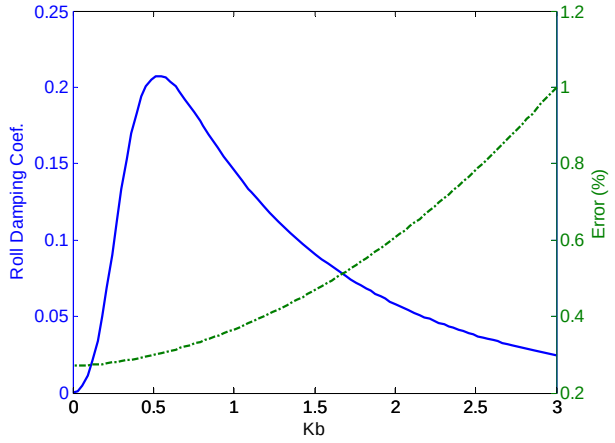

Figure 15 **Error check (roll radiation damping)**
Slika 15 **Provjera greške kod radijacijskog prigušenja ljuljanja**

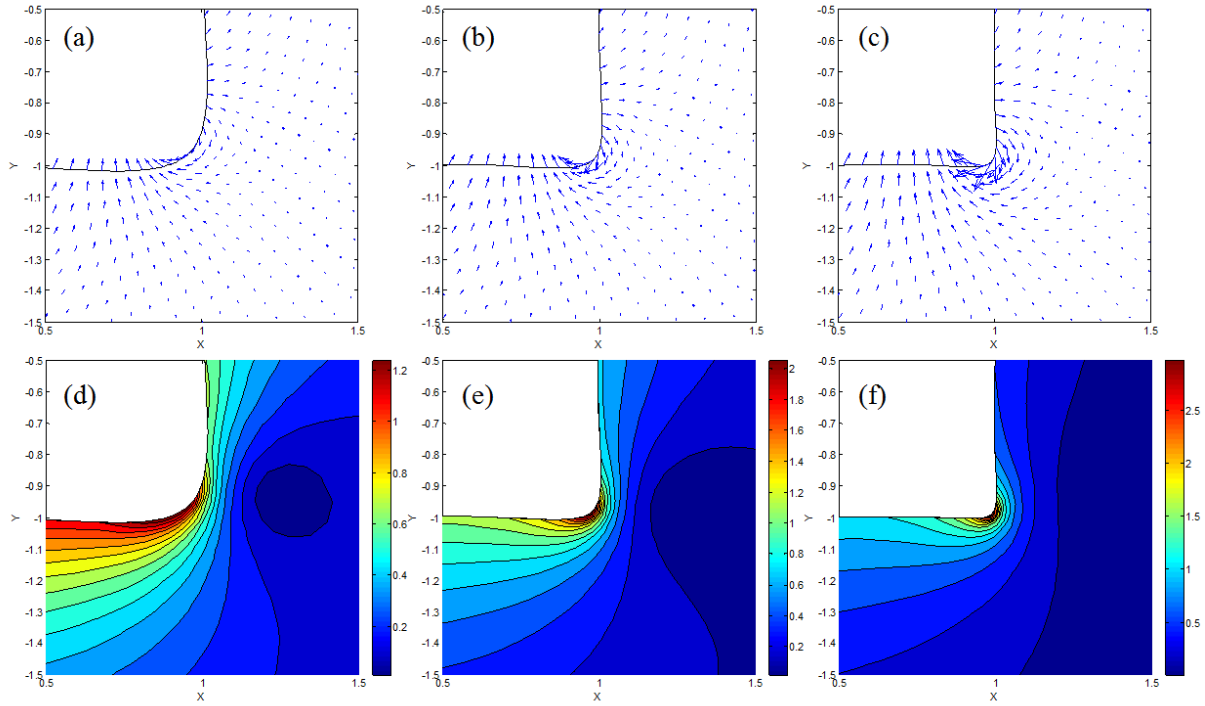

Figure 16 **Velocity vector field and velocity contour at the corner (roll motion), Kb = 0.50, (a,d): N =3, (b,e): N =5, (c,f): N =7**
Slika 16 **Vektorsko polje brzine i izolinije brzine u kutu presjeka kod ljuljanja, Kb = 0.50, (a,d): N =3, (b,e): N =5, (c,f): N =7**

To figure out the reason of the convergence, the flow field with increased *N* around the body was investigated. For fixed *Kb* = 0.5 the velocity field around the corner of the body is illustrated in Figure 16. As the number of terms increased, the magnitude of the velocity around the corner increased. This phenomenon is caused by the geometrical singularity of the corner. It seems that the velocity computed from the velocity potential does not bear the geometric characteristic of the corner because of the ideal fluid assumption. The change in the velocity field for fixed *N* as the value of *Kb* varies was investigated. The results are shown in Figure 17. The *Kb* value at which the velocity reaches maximum was checked in

order to see whether the maximum of the added mass yields at the same *Kb* value. To investigate this, we plotted the velocity contour at the corner for various *Kb*. Figure 18 (b) clearly shows the results.

The velocity field computed from the multipole expansion and that experimentally measured are shown in Figure 19. It can be seen that the agreement gets better when the magnitude of the roll angle is small. It is chiefly due to the fact that the assumption of the boundary value problem was based on the small amplitude motion. In reality the sharp corner will shed vortex due to the viscosity. However, the multipole expansion is based on the inviscid assumption. The experimental results clearly show the existence of vortex.

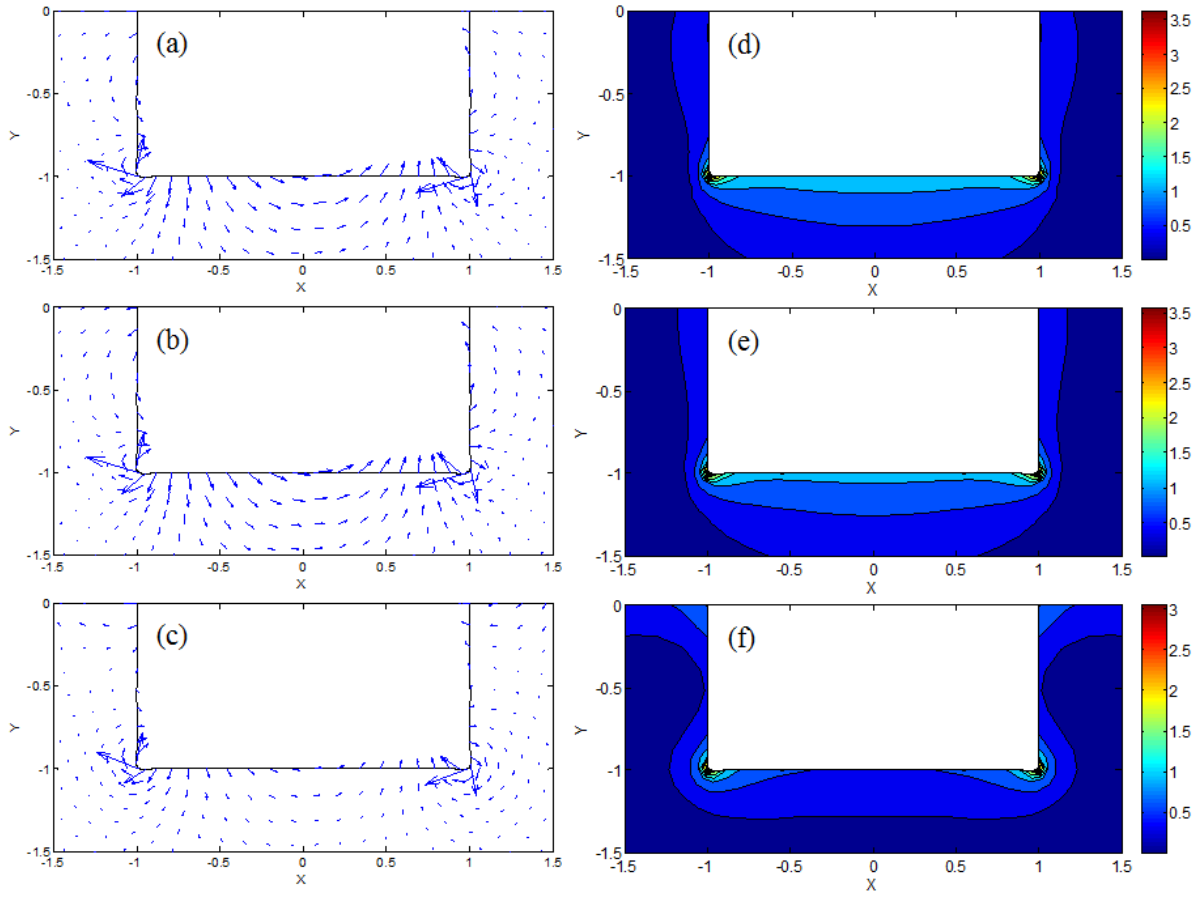

Figure 17 **Velocity vector field and velocity contour, N= 9, (a,d): Kb = 0.10 , (b,e): Kb = 0.25, (c,f): Kb = 1.75**
Slika 17 **Vektorsko polje brzine i izolinije brzine, N= 9, (a,d): Kb = 0.10 , (b,e): Kb = 0.25, (c,f): Kb = 1.75**

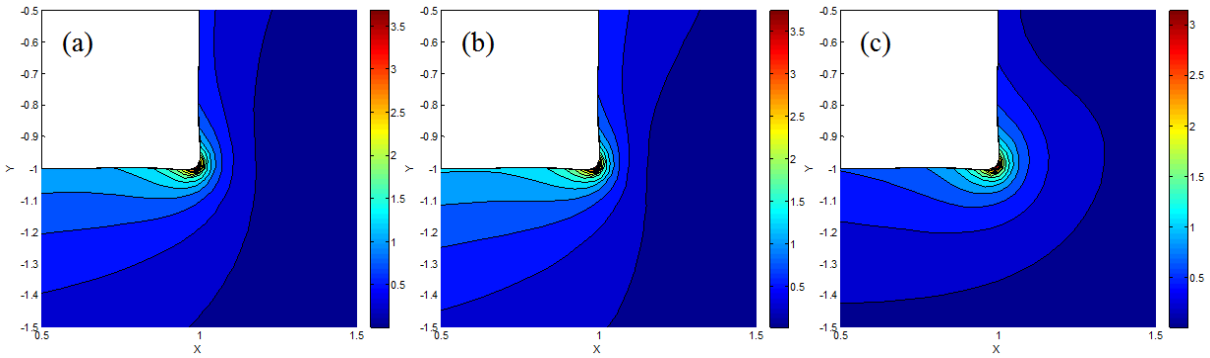

Figure 18 **Velocity contour at the corner, *N*=9, (a): *Kb* = 0.1, (b): *Kb* = 0.25, (c): *Kb* = 1.75**
Slika 18 **Izolinije brzine u kutu presjeka, *N*=9, (a): *Kb* = 0.1, (b): *Kb* = 0.25, (c): *Kb* = 1.75**

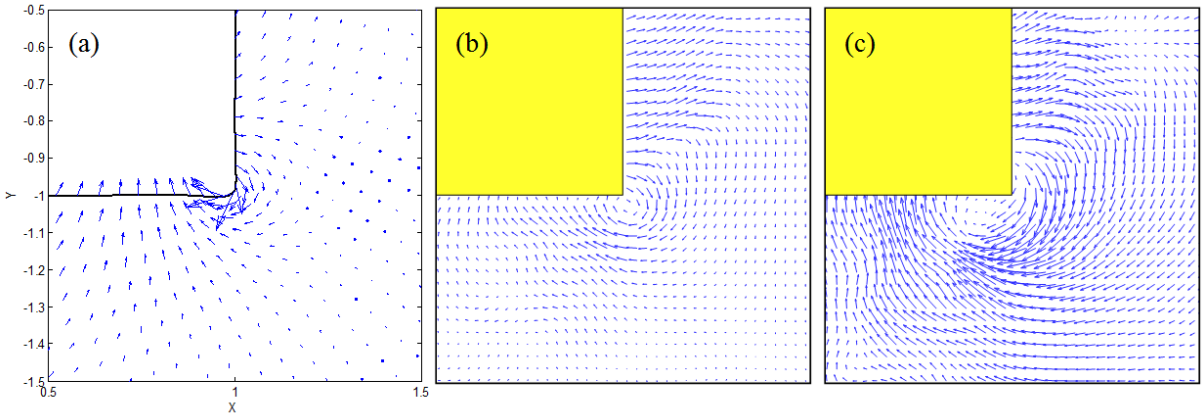

Figure 19 **Flow field at the corner, *Kb* = 0.25 (a): Numerically computed, (b): Experimentally measured ($\theta_A = 2.5°$), (c): Experimentally measured ($\theta_A = 5.0°$)**
Slika 19 **Vektorsko polje brzine u kutu presjeka, Kb = 0.25 (a): numerički izračun, (b): eksperimentalno izmjereno ($\theta_A = 2.5°$), (c): eksperimentalno izmjereno ($\theta_A = 5.0°$)**

5 Conclusions

The present study employed multipole expansion to analyze radiation problem of two-dimensional floating bodies. Ursell was able to calculate the flow field around a two-dimensional circular cylinder with multipole expansions. Tasai introduced conformal mapping to deal with a body with non-circular cross section. Tasai carried out his computation with the 3-parameter Lewis form. Therefore, when the cross section of a floating body deviates from the circular shape, the results get less accurate. In the present study the number of terms in conformal mapping was taken to be greater than 3. The coefficients of the conformal mapping function were taken from the offset of the floating body. This makes it possible to calculate the potential around a rectangular shape cross section. The hydrodynamic coefficients of the rectangular cross section were calculated. The results were compared with those of BEM for various *N* and *Kb*. Calculating velocity field is straight forward with multipole expansion. The corresponding velocity field and velocity contour were presented. When it comes to the sway and heave motion, the convergence of added mass and damping coefficients was very fast with a few terms in mulitpole expansion. However, the calculation of the roll motion needs more terms due to the role of sharp corners of the rectangular cross section. An experiment was carried out to verify the calculated

velocity field. The multipole expansion which is based on inviscid assumption was not able to compute the vortex. However, the advantage of the multipole expansion was demonstrated through this study. First of all, the computation time is extraordinary short when it is compared with other numerical schemes. Secondly, since the velocity potential itself is obtained, the degree of freedom to represent the results is large when it is compared with other CFD codes.

Acknowledgements

This work was supported by the National Research Foundation of Korea (NRF) grant funded by the Korea Government (MEST) (Grant No. 2011-0030670).

List of symbols

ϕ :	velocity potential [m^2/s]
$\mathbf{V}$:	velocity of the body surface [m/s]
$\mathbf{n}$:	unit normal vector on the body surface [-]
K :	wave number [rad/m]
ω :	wave frequency [rad/s]
g :	gravitational acceleration [m/s^2]
c_0, c_m, s_1, s_m :	components of multipole expansion
f :	location of the centre of submerged cylinder [m]
r, θ, r', θ' :	distance and angle from located multipole and mirrored one [m,rad]
a :	radius of cylinder [m]
z, ζ	coordinates of real and mapped plane [-]
B, d	breadth, draft [m]
M, a_{2n-1} :	hull form factor [-]
H_0 :	ratio of breath to draft [-]
σ :	area ratio [-]
x_0, y_0 :	approximated cross section [m]
x_i, y_i :	exact offset of cross section [m]
E :	offset error [m]
X_1, X_2, X_3 :	amplitude of motion (sway, heave, roll) [m]
ϕ_S :	symmetric potential
$\phi_{c0}^S, \phi_{s0}^S, \phi_{2m}^S$:	components of symmetric potential
ϕ_A :	asymmetric potential
$\phi_{c0}^A, \phi_{s0}^A, \phi_{2m}^A$:	components of asymmetric potential
L, B, D :	model length, breadth, depth [m]
a_{ij}, b_{ij} :	added mass, radiation damping
$a_{ij}^{'}, b_{ij}^{'}$:	normalized added mass, radiation damping [-]

References

[1] URSELL, F.: “On the heaving motion of a circular cylinder on the surface of a fluid”, Quarterly Journal of Mechanics and Applied Mathematics, 1949, Vol 2, p.218-231.

[2] TASAI F.: “Formula for calculating hydrodynamic force on a cylinder heaving in the free surface, (N-Parameter Family)”, Technical report, Research Institute for Applied Mechanics, Kyushu University, Japan, 1960, Vol 8, No 31.

[3] EATOCK TAYLOR, R., HU, C.S.: “Multipole expansions for wave diffraction and radiation in deep water”, Ocean Engineering, 1991, Vol. 18, No, 3, p.191-224.

[4] MAVROKOS, S.A., CHATJIGEORGIOU, I.K.: “Hydrodynamic exciting forces on immersed prolate spheroids”, IWWWFB 2012, 2012, Copenhagen, Denmark.

[5] THRONE, R.C.: “Multipole expansions in the theory of surface waves”, Proc. Camb. Phi Soc., 1953, Vol. 49, p.707-716.

[6] ABRAMOWITH, M., STEGUN, I.A.: “Handbook of mathematical functions”, 1965, Dover, New York.

[7] URSELL, F.: “Surface waves on deep water in the presence of a submerged circular cylinder. I, II”, Proceedings of Cambridge Philological Society, 1950, Vol 46, p.141-152, p.153-158.

[8] OGILVIE, T.F.: “First- and second-order forces on a cylinder submerged under a free surface”, Journal of Fluid Mechanics 1963, Vol 16, p.451-472.

[9] LEWIS, F.M.: “The inertia of water surrounding a vibrating ship”, Transactions SNAME, 1929.

[10] NEWMAN, J.N.: “Marine Hydrodynamics”, MIT Press, 1977, Cambridge, Massachusetts.